Numerical simulation study of acoustic waves propagation and streaming using MRT-lattice Boltzmann method

Jaouad Benhamou, Mohammed Jami, Ahmed Mezrhab, Daniel Henry, Valéry Botton

▶ **To cite this version:**

Jaouad Benhamou, Mohammed Jami, Ahmed Mezrhab, Daniel Henry, Valéry Botton. Numerical simulation study of acoustic waves propagation and streaming using MRT-lattice Boltzmann method. International Journal for Computational Methods in Engineering Science and Mechanics, 2022, pp.1-14. 10.1080/15502287.2022.2050844 . hal-03622040

HAL Id: hal-03622040
https://hal.science/hal-03622040

Submitted on 28 Mar 2022

HAL is a multi-disciplinary open access archive for the deposit and dissemination of scientific research documents, whether they are published or not. The documents may come from teaching and research institutions in France or abroad, or from public or private research centers.

L'archive ouverte pluridisciplinaire **HAL**, est destinée au dépôt et à la diffusion de documents scientifiques de niveau recherche, publiés ou non, émanant des établissements d'enseignement et de recherche français ou étrangers, des laboratoires publics ou privés.

Numerical simulation study of acoustic waves propagation and streaming using MRT-lattice Boltzmann method

Jaouad Benhamou[1*], Mohammed Jami[1], Ahmed Mezrhab[1], Daniel Henry[2], Valéry Botton[2]

[1]Laboratoire de Mécanique & Energétique, Faculté des Sciences, Université Mohammed Premier, 60000 Oujda, Morocco.

[2]Laboratoire de Mécanique des Fluides et d'Acoustique, CNRS/Université de Lyon, Ecole Centrale de Lyon/Université Lyon 1/INSA Lyon, ECL, 36 Avenue Guy de Collongue, 69134 Ecully Cedex, France.

*Corresponding author: jaouad1994benhamou@gmail.com

Abstract

This paper presents a numerical investigation of the propagation of acoustic waves generated by a linear acoustic source using the lattice Boltzmann method (LBM). The main objective of this study is to compute the sound pressure and acoustic force produced by a rectangular sound source located at the center of the west wall of a rectangular cavity, filled with water. The sound source is discretized into a set of point sources emitting waves according to the acoustic point source method. The interference between the generated cylindrical waves creates an acoustic beam in the cavity. An analytical study is carried out to validate these numerical results. The error between the numerical and analytical calculations of the wave propagation is also discussed to confirm the validity of the numerical approach. In a second step, the acoustic streaming is calculated by introducing the acoustic force into the LBM code. A characteristic flow structure with two recirculating cells is thus obtained.

Keywords: Acoustic waves, Acoustic streaming, Lattice Boltzmann method, Acoustic force, Acoustic point source.

1. Introduction

Lattice Boltzmann method (LBM) is a numerical approach, which is derived from the kinetic theory of gases and cellular automata [1–3]. This approach is generally different from those traditionally used in numerical computations, as in computational fluid dynamics (CFD). Instead of relying on the Navier-Stokes equations, the LBM is based on the Boltzmann statistical equation [4,5]. In recent years, numerical simulation of acoustic waves by the LB approach has become a well-known research topic in the literature. For example, several studies have been performed to investigate different types of waves using lattice Boltzmann tools, such as elastic waves [6,7], shock waves [8,9], aeroacoustic waves [10–12], and sound waves [13–15].

One of the advantages of using the LBM in acoustics is that the sound waves can easily be generated using a simple boundary condition. For example, Haydock and Yeomans [16] have shown that the lattice Boltzmann method can be applied to model the acoustic streaming produced by a traveling

wave by adding a sine term to the bounce-back boundary condition. In the same way, Shan et al. [17] published a comprehensive paper on the use of the axisymmetric lattice Boltzmann method, with the Bouzidi–Firdaouss–Lallemand (BFL) boundary condition, to simulate the ultrasounds generated by a focused transducer [18]. Here, the sound waves are generated by using the point source method [15,19–21]. The main idea of this approach is to generate the waves by a harmonic function of the fluid density oscillating at the boundary around the equilibrium density.

There are many applications of acoustic waves, especially ultrasound waves. For example, in medicine, the signals created can be used for diagnostic or therapeutic purposes [22,23]. In daily life, the waves can be used for cleaning [24]. In the industrial sector, the acoustic waves generated by a piezoelectric transducer can be used to purify photovoltaic silicon [25]. This purification is obtained through the flow created in the fluid by the propagation of the acoustic waves (acoustic streaming). This streaming is due to the natural attenuation in the fluid of the acoustic wave generated by the transducer vibration. Numerically, it is generally generated by introducing the force induced by the waves (acoustic force) in the numerical code. For CFD methods, the force is added to the Navier-Stokes equations [26], whereas for LBM methods, there are several models for introducing such external force [27]. In any case, the calculation of the acoustic force is a key ingredient for all numerical methods to study acoustic streaming.

There are two types of acoustic streaming: Eckart streaming [28] and Rayleigh streaming [29]. In the first case, the fluid motion is created within the fluid bulk by the Reynolds tensions resulting from the propagation of the attenuated acoustic wave, and, in the second case, the Reynolds tensions act in the acoustic boundary layers which develop along the solid walls. The lattice Boltzmann method has been used to study acoustic streaming for many years. For example, Stansell and Greated [30] numerically studied the acoustic streaming resulting from the interaction of acoustic waves with no-slip boundaries in a 2D pipe using the lattice gas automaton fluid modeling method. Haydock and Yeomans [31] used the LB approach to study the acoustic streaming phenomena induced by the interaction of a sound wave with a boundary. They also modeled the attenuation-driven acoustic streaming produced by an acoustic wave using the LB simulations [16]. Rafat et al. [32] used the lattice Boltzmann numerical simulations to study the acoustic streaming in standing wave tubes.

Compared with these previous works, the focus of our study is different: we are interested in the streaming flow generated by an extended ultrasound source, in view of engineering applications. Our situation approximates those presented in reference [25]. In this work, the acoustic waves are generated experimentally by a circular piezoelectric transducer and are numerically taken into account in a CFD code by calculating the acoustic pressure field obtained as the added contributions of the discretized circular source into small elements (Rayleigh's integral). In our 2D approximation, the circular ultrasound source is replaced by a rectangular source, which is placed at the center of the west wall of a rectangular cavity filled with water. Our idea is to calculate the acoustic force induced by the waves directly with the LB method and then to introduce this force in the LBM calculation to get the streaming. For that, different steps are necessary. The extended source has first to be discretized into a set of point sources, which are modeled with the acoustic point source method. Then, the travel of the waves, emitted by the point sources, across the cavity, is calculated by the LB method, allowing to get the pressure and velocity fields. The next step is to determine the acoustic force. Two different methods are tested and compared. The first method, which uses the plane wave approximation, is based on the calculation of the mean squared pressure, as mentioned in references [25,26]. The second method calculates the force as the mean spatial variation of the Reynolds stress, using the

mathematical formulation given in references [33,34]. Finally, once the acoustic forces are available, the streaming induced by such forces is calculated by the LB method.

2. D2Q9-MRT lattice Boltzmann method

The multiple relaxation time lattice Boltzmann method (MRT) is more stable and precise than the simple relaxation model (SRT) to study the propagation of the acoustic waves [19]. For this reason, the D2Q9-MRT scheme is chosen to study the physical acoustic problem presented in this article. The evolution of the fluid using the MRT approach is described by the following lattice Boltzmann equation [4,35–38]:

$$f_i(x_i + c_i\delta t, t + \delta t) - f_i(x_i, t) = -\Lambda\ [f_i - f_i^{eq}], \tag{1}$$

where f_i and f_i^{eq} represent the distribution functions and the equilibrium distribution functions, respectively. δt is the LBM time step ($\delta t = 1$ in the lattice Boltzmann units), Λ is the collision matrix and c_i denote the lattice velocities of the D2Q9 scheme (Fig. 1):

$$c_i = \begin{cases} (0,0) & i = 0 \\ (1,0)\mathrm{c}, (0,1)c, (-1,0)\mathrm{c}, (0,-1)\mathrm{c} & i = 1,..,4 \\ (1,1)\mathrm{c}, (-1,1)c, (-1,-1)\mathrm{c}, (1,-1)\mathrm{c} & i = 5,..,8 \end{cases} \tag{2}$$

where c is the LBM speed between two successive nodes of the lattice. Typically, it is equal to 1 in the LBM units.

The equilibrium distribution function is defined as [4,39,40]:

$$f_i^{eq} = w_i\rho \left[1 + \frac{1}{c_s^2}\left(\vec{c}_i.\vec{V}\right) + \frac{1}{2c_s^4}\left(\vec{c}_i.\vec{V}\right)^2 - \frac{1}{2c_s^2}\left|\vec{V}\right|^2\right] \tag{3}$$

where w_i are the discretization weights, ρ is the fluid density, c_s is the speed of sound ($c_s = 1/\sqrt{3}$ in LBM units) and $\vec{V}$ is the macroscopic velocity vector ($\vec{V} = (\vec{u}, \vec{v})$). For the D2Q9 model, the weight coefficients are $w_0 = 4/9$, $w_1 = w_2 = w_3 = w_4 = 1/9$ and $w_5 = w_6 = w_7 = w_8 = 1/36$ [4,41].

For the LBM-MRT model, the collision matrix is generally presented as follows [36]:

$$\Lambda = M^{-1}\, S\, M, \tag{4}$$

where S, M and M^{-1} are the relaxation matrix, the transformation matrix and its inverse matrix, respectively.

Using the following linear transformations, $m = Mf$ and $m^{eq} = Mf^{eq}$, the Boltzmann equation becomes:

$$f_i(x_i + c_i\delta t, t + \delta t) - f_i(x_i, t) = M^{-1}S[\, m_i^{eq} - m_i]. \tag{5}$$

For the MRT-D2Q9 scheme, the matrix M is a (9×9) matrix. According to [4], it is given by:

$$M = \begin{pmatrix} 1 & 1 & 1 & 1 & 1 & 1 & 1 & 1 & 1 \\ -4 & -1 & -1 & -1 & -1 & 2 & 2 & 2 & 2 \\ 4 & -2 & -2 & -2 & -2 & 1 & 1 & 1 & 1 \\ 0 & 1 & 0 & -1 & 0 & 1 & -1 & -1 & 1 \\ 0 & -2 & 0 & 2 & 0 & 1 & -1 & -1 & 1 \\ 0 & 0 & 1 & 0 & -1 & 1 & 1 & -1 & -1 \\ 0 & 0 & -2 & 0 & 2 & 1 & 1 & -1 & -1 \\ 0 & 1 & -1 & 1 & -1 & 0 & 0 & 0 & 0 \\ 0 & 0 & 0 & 0 & 0 & 1 & -1 & 1 & -1 \end{pmatrix} \quad (6)$$

The matrix S is a diagonal matrix. It defines the nine relaxation times s_i of the associated physical quantities calculated by the D2Q9 model:

$$S = \mathrm{diag}(s_0, s_1, s_2, s_3, s_4, s_5, s_6, s_7, s_8). \quad (7)$$

The relaxation time values used in this work are those described in [4]: $s_1 = s_2 = 1.4$, $s_0 = s_3 = s_5 = 1$, $s_4 = s_6 = 1.2$ and $s_7 = s_8 = 1/(3\nu + 0.5)$, where ν is the LBM kinematic viscosity.

m is the vector of the nine moments given by the D2Q9 lattice. These moments correspond to the fluid density (ρ), energy (e), energy square (ε), momentum ($j = (j_x, j_y)$), energy flux (q_x, q_y), and the two moments linked to the diagonal (p_{xx}) and off-diagonal (p_{xy}) components of the stress tensor [4,38]:

$$m = \left(\rho, e, \varepsilon, j_x, q_x, j_y, q_y, p_{xx}, p_{xy}\right)^T, \quad (8)$$

where the superscript T indicates that we consider the transposed matrix.

m^{eq} is the vector of the equilibrium moments [42]:

$$\begin{aligned} m_0^{eq} &= \rho \\ m_1^{eq} &= -2\rho + \frac{3}{\rho}(j_x^2 + j_y^2) \\ m_2^{eq} &= \rho - \frac{3}{\rho}\left(j_x^2 + j_y^2\right) \\ m_3^{eq} &= j_x \\ m_4^{eq} &= -j_x \\ m_5^{eq} &= j_y \\ m_6^{eq} &= -j_y \\ m_7^{eq} &= \frac{1}{\rho}(j_x^2 - j_y^2) \\ m_8^{eq} &= \frac{1}{\rho} j_x j_y \end{aligned} \quad (9)$$

After calculating the nine distribution functions by numerically solving the Boltzmann equation, the macroscopic quantities ρ, j_x and j_y can be determined by the following equations [4]:

$$\rho = \sum_{i=0}^{8} f_i, \quad j_x = \rho u = \sum_{i=0}^{8} f_i \, c_{ix} \text{ and } j_y = \rho v = \sum_{i=0}^{8} f_i \, c_{iy}, \quad (10)$$

where c_{ix} and c_{iy} are the Boltzmann velocities along the x and y axes, respectively.

To produce the acoustic streaming, the force induced by the propagation of the sound waves in water is introduced into the LBM code. The Shan and Chen model [43,44] and the model proposed by Luo [27] are the most popular models for implementing an external force in the LB method. The first model consists in modifying the amount of motion $j(x, y)$ in the following way:

$$j(x,y) = \sum f_i \, c_i + \frac{\delta t \, F_{ac}}{2} \tag{11}$$

where F_{ac} is the acoustic force.

For the second model, the external force is discretized and then directly added to the Boltzmann equation (Eq. (5)). The discretized force can be given as [45]:

$$F_i = w_i c_i \, F_{ac} \, c_s^{-2}, \tag{12}$$

Then, Eq. (5) becomes [42]:

$$f_i(x_i + c_i \delta t, t + \delta t) - f_i(x_i, t) = M^{-1} S\left[m_i^{eq} - m_i\right] + \delta t \, F_i. \tag{13}$$

The calculation of the acoustic force will be detailed in section 5 and its implementation in our LBM code is carried out according to the Luo model (Eq. (13)).

3. Boundary conditions

The boundary conditions used in this work are the bounce-back and characteristic boundary conditions.

The bounce-back boundary conditions are applied to define the unknown distribution functions at the solid boundary. The main idea is to calculate the unknown f_i from the known functions by the following equation [4,21]:

$$f_i(\vec{x}_B, t) = f_{\bar{i}}(\vec{x}_B, t) \tag{14}$$

where $f_i(\vec{x}_B, t)$ is an unknown distribution function at the wall node ($\vec{x}_B$) and $f_{\bar{i}}(\vec{x}_B, t)$ is the known function at the opposite direction of $f_i(\vec{x}_B, t)$.

The characteristic boundary conditions (CBC) are one of the most used conditions in the lattice Boltzmann method for absorbing the sound wave at boundaries [46]. The origin and implementation of these conditions are discussed in detail in the references [5,47,48]. Here, only the calculation of the CBCs at a vertical wall that is at a given position in x (x −boundary) is proposed.

The simplest way to implement the characteristic boundary conditions in the LBM code is to directly replace the distribution function f_i at the boundary with the equilibrium distribution function f_i^{eq}:

$$f_i(\vec{x}_B, t) = f_i^{eq}(\vec{x}_B, t). \tag{15}$$

f_i^{eq} is expressed as a function of the density (ρ_D) and the velocities (u_D, v_D) (Dirichlet values), which can be calculated at the x −boundary by solving the following equation [5]:

$$\frac{\partial \vec{U}}{\partial t} = -\mathrm{P_x}^{-1} L_x' - \gamma \mathrm{Y} \frac{\partial \vec{U}}{\partial y} \tag{16}$$

where $\overrightarrow{U}$ is the fluid variable vector $\overrightarrow{U} = (\rho, u, v)^T$ and γ is a constant that is set to unity ($\gamma = 1$) as in reference [5].

Y is a (3×3) matrix. It is expressed as:

$$\mathrm{Y} = \begin{pmatrix} v & 0 & \rho \\ 0 & v & 0 \\ c_s^2/\rho & 0 & v \end{pmatrix}, \tag{17}$$

$\mathrm{P}_{\mathrm{x}}^{-1}$ is also a matrix, function of the speed of sound and density:

$$\mathrm{P}_{\mathrm{x}}^{-1} = \begin{pmatrix} \frac{1}{2c_s^2} & 0 & \frac{1}{2c_s^2} \\ -\frac{1}{2\rho c_s} & 0 & \frac{1}{2\rho c_s} \\ 0 & 1 & 0 \end{pmatrix}. \tag{18}$$

L'_x is a modified characteristic vector deduced from the characteristic vector L_x in such a way to attenuate the incoming waves at the boundary and then avoid reflection:

$$L'_{x,i} = \begin{cases} L_{x,i} & \text{for outgoing waves} \\ 0 & \text{for incoming waves} \end{cases} \tag{19}$$

Finally, the components of L_x are:

$$L_x = \begin{cases} L_{x,1} = (u - c_s)\left[c_s^2 \frac{\partial \rho}{\partial x} - c_s \rho \frac{\partial u}{\partial x}\right] \\ L_{x,2} = u \frac{\partial v}{\partial x} \\ L_{x,3} = (u + c_s)\left[c_s^2 \frac{\partial \rho}{\partial x} + c_s \rho \frac{\partial u}{\partial x}\right] \end{cases} \tag{20}$$

The development of the matrix calculation expressed by Eq. (16) leads to the following three differential equations for the density and the velocities along the x and y axes:

$$\frac{\partial \rho}{\partial t} = -\left(\frac{L'_{x,1}}{2c_s^2} + \frac{L'_{x,3}}{2c_s^2} + v \frac{\partial \rho}{\partial y} + \rho \frac{\partial v}{\partial y}\right), \tag{21}$$

$$\frac{\partial u}{\partial t} = -\left(-\frac{L'_{x,1}}{2\rho c_s} + \frac{L'_{x,3}}{2\rho c_s} + v \frac{\partial u}{\partial y}\right), \tag{22}$$

$$\frac{\partial v}{\partial t} = -\left(L'_{x,2} + \frac{c_s^2}{\rho} \frac{\partial \rho}{\partial y} + v \frac{\partial v}{\partial y}\right). \tag{23}$$

The discretization of these three equations is done using the finite difference method. For example, for Eq. (21), the spatial derivative at the vertical walls is given using the one-sided second-order finite difference approximations [5]:

$$\frac{\partial \rho}{\partial y} = \frac{\overline{+}\, 3\rho(y) \pm 4\, \rho(y \pm \delta y)\, \overline{+}\, \rho(y \pm 2\delta y)}{2\delta y}. \tag{24}$$

On the other hand, inside the computational domain, the second-order central difference approximation is used:

$$\frac{\partial \rho}{\partial y} = \frac{\rho(y + \delta y) - \rho(y - \delta y)}{2\delta y}, \tag{25}$$

where δy is the space step along y ($\delta y = 1$).

To advance in time, the forward Euler method can be applied [5]. As an example, for ρ, this leads to:

$$\rho(t + \delta t) = \rho(t) + \delta t \frac{\partial \rho}{\partial t}. \tag{26}$$

Solving numerically Eqs. (21-23) will then give ρ_D, u_D and v_D at the boundary. The values of these variables thus obtained are integrated into Eq. (3) to calculate the corresponding equilibrium distribution function.

4. Lattice Boltzmann Units

The conversion between the physical and LBM units is very important, especially when we want to deal with a real physical problem using the lattice Boltzmann method. The simplest way is to perform this conversion between the two sets of units by using reference physical quantities for length, time, and density. We will use the spacing of the nodes Δx (m), the physical time step Δt (s) and the mean density of the fluid ρ (Kg/m^3) [19,49]. With this choice, $\Delta x_{lbm} = \delta x = 1$, $\Delta t_{lbm} = \delta t = 1$ and $\rho_{lbm} = 1$. The physical speed of sound (c_{ph}) and viscosity (ν_{ph}) can also be linked to those of the LBM by the following equations:

$$c_{ph} = \frac{\Delta x}{\Delta t} c_{lbm}, \tag{27}$$

$$\nu_{ph} = \frac{\Delta x^2}{\Delta t} \nu_{lbm}. \tag{28}$$

As the physical quantities in Eqs. (27) and (28) are known and that c_{lbm} is typically chosen as $1/\sqrt{3}$ for the D2Q9 model ($c_{lbm} = c_s$), a possibility is to fix a value for ν_{lbm} and to use these two equations to obtain Δx and Δt:

$$\Delta x = \frac{\nu_{ph}}{\nu_{lbm}} \frac{c_{lbm}}{c_{ph}}, \tag{29}$$

$$\Delta t = \frac{\nu_{ph}}{\nu_{lbm}} \left(\frac{c_{lbm}}{c_{ph}}\right)^2. \tag{30}$$

Another choice was done here. For the study of acoustic problems, an important physical quantity is the physical frequency of the wave ($f_{ph} = 200$ kHz in our work), from which the period of the wave ($T_{ph} = 5 \times 10^{-6}$ s) and the wavelength ($\lambda_{ph} = 7.4 \times 10^{-3}$ m) can be deduced. To have a precise calculation of the waves in the cavity, we decided to have at least 20 Δx in a wavelength, which led us to choose $\Delta x = 3.2 \times 10^{-4}$ m and Δt was deduced from Eq. (27) ($\Delta t = 1.248 \times 10^{-7}$ s). With this choice of Δx and Δt, the LBM period and wavelength can be obtained as $T_{lbm} = T_{ph}/\Delta t = 40.064$ and $\lambda_{lbm} = \lambda_{ph}/\Delta x = 23.125$, respectively. Note that with the choices made here, the LBM viscosity is not an adjustable parameter and must be obtained from Eq. (28).

The purpose of this work is to study the propagation of sound waves in water. Some of the physical and LBM parameters used in our simulations are given in Table 1.

5. Results and Discussion

The sound waves are generated by a rectangular acoustic source located at the center of the west wall of a rectangular cavity of height $H = 10$ cm and length $L = 15$ cm filled with water (see Fig. 2). The size of the acoustic source is 3.33 cm (i.e. H/3). The waves are emitted by the source with a physical frequency (f_{ph}) of 200 kHz and will travel towards the east wall of the cavity. To avoid the reflection of the sound waves at this boundary, the characteristic boundary conditions presented in section 3 are used. For the other walls, the usual bounce-back boundary conditions are applied.
With the choice of $\Delta x = 3.2 \times 10^{-4}$ m and $\Delta t = 1.248 \times 10^{-7}$ s presented in section 4, the numbers of nodes along the length and height of the cavity are 469 (from 0 to $N_x = 468$) and 313 (from 0 to $N_y = 312$), respectively, which also gives 105 (from 0 to $N_s = 104$) nodes along the acoustic source. Note also that the number of wavelengths contained in the length will then be about 20, and 1000 time iterations will correspond to about 25 wave periods.

Numerically, the acoustic source is discretized into a set of point sources, and each source is modeled by the following linear density equation [15,19,39]:

$$\rho = \rho_0 + \rho' \tag{31}$$

where ρ_0 is the equilibrium density, which is equal to 1 in the LBM units, and ρ' is the off-equilibrium density. For the case of circular waves, the acoustic density ρ' can take the following form:

$$\rho' = A\ sin\ (\frac{2\pi}{T} t) \tag{32}$$

where $A, t,$ and T are the amplitude of the point acoustic source, the time, and the harmonic period, respectively. In the LBM units, t represents the number of iterations in the LBM code. The amplitude value of the sound source must be sufficiently low to avoid the non-linear effects in the propagation of the acoustic waves [19]. In this study, the amplitude generally used ($A = 0.01$) is that mentioned in references [15,21].

5.1. Test cases

To validate our LBM code, we first studied the acoustic wave emitted by a point source located at the center of a square cavity (10 cm × 10 cm) filled with water. The characteristics of this test case are similar to those described before for the rectangular cavity. In particular, a wave absorbing boundary condition is applied at the east wall. We also choose $f_{ph} = 200$ kHz, so that $\lambda_{ph} = 7.4 \times 10^{-3}$ m. Δx and Δt are chosen as mentioned before so that 313 nodes must be taken along each axis x and y and a wavelength will correspond to about 23 nodes. The results are illustrated in Fig. 3. For a small number of iterations equal to 200 (Fig. 3a), the waves propagate as circles in the cavity without still reaching the walls. When the iterations become more important (400 for example), the waves are absorbed by the east wall and reflected by the other walls of the cavity. The interference between the reflected waves and those emitted by the source is then well observed (Fig. 3b).

Another test case is performed, which also corresponds to a wave emitted by a point source at the center of a square cavity. The configuration proposed by Salomons et al. [15], however, has different characteristics. The cavity is filled with air and has bounce-back boundary conditions applied on all its walls, and the calculations were performed with a LBM period and a viscosity of 40 and 0.06,

respectively. The results obtained with our LBM code for an iteration number equal to 1600 are favorably compared with those found by Salomons et al. [15] (see Fig. 4).

5.2. Wave propagation

After these different test cases, we now consider the physical problem depicted in Fig. 2. The sound waves are here generated by a rectangular acoustic source placed on the west wall of the cavity. The discretization of this rectangular source gives 105-point sources placed on the corresponding 105 nodes of the LBM lattice. Fig. 5 shows the numerical results calculated by the D2Q9-LBM scheme. These results are obtained after 1400 iterations, which, for a LBM period of about 40, correspond to 35 wave periods. The generated waves propagate throughout the enclosure in the form of plane waves. These plane waves are directed towards the east wall of the cavity where they are absorbed. The corresponding acoustic beam is rather intense close to the source, in the zone at mid-height in front of the source. The global shape of the waves is cylindrical in the far-field (for example beyond mid-length), but closer to the source in the near-field the shape becomes flat in the zone in front of the source, with stronger curvatures above and below this zone.

Salomons et al. [15] have shown that high values of the fluid viscosity can cause strong sound dissipation. For negligible thermal effects (which is a good approximation for water [25]), the dissipation is given by the following equation:

$$\alpha = \frac{1}{2}\,\omega^2 \left(\frac{4}{3}\nu + \nu_B\right) c_s^{-3} \tag{33}$$

where α is the spatial attenuation coefficient and ν_B is the bulk viscosity, generally taken proportional to the viscosity (for water, $\nu_B = 3\,\nu$) [25,50].

As shown before, the LBM viscosity (ν) for water can be easily determined using Eq. (28). For the conditions used in this work, the value of the LBM viscosity is about 1.21×10^{-6}. This value was used in Figs. 3 and 5. Let us note that this viscosity is very low so that it will not cause a strong attenuation. It should be interesting to study the effect of the viscosity on the propagation of the sound waves and for that to compute new cases with stronger viscosity ($\nu = 0.01$ and 0.06), and to see how the waves are thus dissipated. The results are shown in Fig. 6, which depicts the longitudinal profiles of the density obtained for the different values of the LBM viscosity. It should be first noted that, due to the diffraction effect, there is a decrease of the wave amplitude, visible in the far-field, even with no viscosity effect. The result obtained for $\nu = 1.21 \times 10^{-6}$ can be considered as typically representing this effect due to diffraction. When the viscosity is increased up to 0.01, an extra-dissipation due to viscosity is effective and can be observed on the density profile, but it still remains weak. It is only with the higher value of the viscosity ($\nu = 0.06$) that the dissipation becomes important, giving a quite strongly attenuated density profile.

Here, we can mention one of the advantages of the MRT model compared to the SRT model. For the SRT scheme, the viscosity chosen in the LBM calculations must be greater than 0.01 to avoid instability effects [15], whereas, for the MRT model, there is no constraint on the viscosity, and viscosity values far below 0.01 can thus be used.

Our numerical results can be validated using the analytical solution of the equation of cylindrical waves. For a single sound point source, this analytical solution is given by the real part of the following expression [15,19,21]:

$$\rho'(r,t) = BH_0^{(2)}(kr)e^{j\omega t}, \tag{34}$$

where $H_0^{(2)}$ is the Hankel function of order zero and second kind, r is the distance to the sound source, k is the wavenumber and B is a constant. This expression using a real value of k does not take into account the spatial sound attenuation effect. The mathematical expressions of the Henkel function and the constant B are discussed in reference [19].

In the case of a rectangular sound source, the sum of the density fields given by each point source must be made:

$$\rho_s(r,t) = \sum_{i=1}^{N_s} \rho_i(r,t), \tag{35}$$

where N_s is the number of acoustic sources ($N_s = 104$ in our case).

The analytical result thus obtained is illustrated in Fig. 7, which gives the density field in the cavity at a time corresponding to 1400 time steps, to compare with the numerical result shown in Fig. 5. As the analytical result does not involve sound attenuation, the comparison makes sense only with the numerical result obtained for small viscosity (as $\nu = 1.21 \times 10^{-6}$ in Fig. 5). There is a good global agreement between the analytical and numerical results. Note however that, due to the reflection of the waves on the north and south walls in the numerical computations, interference occurs and modifies the shape of the waves close to these walls compared to the analytical results. To show more clearly the agreement, the analytical and numerical density profiles along the x-axis obtained from the results presented in Fig. 7 and Fig. 5, respectively, are plotted in Fig. 8. These profiles are very similar, although a small difference between them can be noted. This difference can be highlighted by calculating the absolute error Ea, which is determined as the difference between the numerical (ρ_{Num}) and analytical (ρ_{Anl}) densities obtained at each LBM node point [21]:

$$Ea = |\rho_{Anl} - \rho_{Num}|. \tag{36}$$

Fig. 9 presents the absolute error variation along the x-axis. It oscillates between 0 and about 4×10^{-4} along this axis, except in the vicinity of the sound source where it takes a larger amplitude. The maximum error found along the x-axis (8×10^{-4}) can be already considered as very small, indicating that the numerical results are very close to those calculated analytically. The mean absolute error (Em) along the x-axis can also be calculated:

$$Em = \frac{1}{N}\sum_{i=0}^{N} Ea_i, \tag{37}$$

where N is the number of points along the x-axis. We obtain $Em = 1.78 \times 10^{-4}$. These good comparisons with the analytical calculations indicate the validity and accuracy of our numerical approach.

5.3. Acoustic force

It is now interesting to evaluate the acoustic force induced by the attenuated wave as it is responsible for the development of acoustic streaming. The acoustic force can be determined from the acoustic pressure field generated by the transducer. In the particular case of progressive sinusoidal plane waves, the force can take the following form [25,26]:

$$F_{ac} = \frac{\alpha p_{ac}^2}{\rho c_s^2}, \tag{38}$$

where c_s, α, ρ, and p_{ac} are the speed of the sound, the acoustic attenuation coefficient, the fluid density, and the acoustic pressure amplitude, respectively. The attenuation coefficient has been given in Eq. (33). The acoustic pressure is obtained from the off-equilibrium density ρ' as $p' = \rho' c_s^2$, i.e. $p' = (\rho - \rho_0)c_s^2$. Its amplitude can be determined from its rms-value. Indeed, for a pressure wave expressed as $p' = p_{ac}\, cos(\omega t - kx)$, the amplitude p_{ac} is:

$$p_{ac} = \sqrt{2\,\langle p'^2 \rangle}\,. \tag{39}$$

To calculate the average of the squared acoustic pressure $\langle p'^2 \rangle$, the generated acoustic waves must be well established throughout the cavity. In our situation, the waves reach the east wall after 800 iterations ($t = 800\,\Delta t$), indicating that the mean value has to be calculated on a time interval chosen at least beyond that time.

The acoustic force can also be calculated as the spatial variation of the Reynolds stress, as presented in the references [26,33,34]:

$$F_{ac,i} = -\rho \nabla.\left(\langle u_{ac,i}\, \vec{u}_{ac} \rangle\right), \quad \text{for } i = 1 \text{ and } 2 \tag{40}$$

where $\vec{u}_{ac}$ is the acoustic velocity. The derivatives that are needed in that case are calculated using the finite differences approximation. At the boundaries, a one-sided second-order approximation is used, whereas, for points outside the edges, a second-order central scheme is applied [5].

The acoustic forces have been calculated using Eq. (38) or Eq. (40). The time averages that are needed, either for p_{ac} in Eq. (38) or for $\vec{u}_{ac}$ in Eq. (40), have been performed between the iterations 1000 and 1400, i.e. on a time interval of about 10 periods. Different tests have been carried out corresponding to different values of the LBM viscosity ν, i.e. also different values of the acoustic attenuation coefficient α. From these tests, we have found that the two forces have similar intensities and spatial variations when the LBM viscosity is quite high. For example, the force fields obtained for $\nu = 0.06$ with Eq. (38) and Eq. (40) are presented in Figs. 10 and 11, respectively. From these figures, we can see that the force is more important closer to the source where the waves have larger intensities and weakens away from the source under the effect of sound diffraction and acoustic attenuation. Note that differences between the two forces appear in the spatial variations in the near field, very close to the source. Due to the spatial derivatives involved, the force field obtained from Eq. (40) is also less smooth. The good agreement between the two acoustic force formulas, however, can be shown on transverse profiles taken at different positions along the x-axis, i.e. the sound propagation direction. These profiles, taken at $x = L/3$, $L/2$, and $2L/3$, are shown in Fig. 12. We can see that in this case, where $\nu = 0.06$, there is a rather good match between the profiles obtained by either Eq. (38) or Eq. (40).

As mentioned before, the LBM viscosity corresponding to the physical case of wave propagation in water is $\nu = 1.21 \times 10^{-6}$. For this small value of ν, however, the two expressions of the force are not equivalent. We have first to remember that the source of the streaming, and then also of the acoustic force, is the sound attenuation, quantified by the acoustic attenuation coefficient α. This coefficient is explicitly present in the force expression given by Eq. (38), which will then give the right force amplitude and level of streaming, even if the very low dissipation effect is not perfectly taken into account in the calculation of the wave propagation. In contrast, the attenuation effect is only implicitly

taken into account in Eq. (40) through the attenuation of the wave, more precisely the attenuation of the acoustic velocities. If strong attenuation is effective (as for $\nu = 0.06$), this attenuation effect will strongly affect the calculated acoustic velocities and the use of Eq. (40) for the force calculation can be appropriate. For low attenuation, however, the effect on the acoustic velocities is so weak that it is difficult to precisely take it into account in a numerical simulation and the use of Eq. (40) becomes inappropriate. This is the case for the very low acoustic attenuation ($\alpha = 3.35 \times 10^{-7}$) effective in water at $f = 200$ kHz ($\nu = 1.21 \times 10^{-6}$), for which only Eq. (38) can be used with confidence.

5.4. Streaming

Our final objective is now to use the LB method to calculate the streaming induced by the wave in the cavity filled with water, using the acoustic force field calculated from the wave propagation, as shown just above. Let us first recall that Fig. 6 shows that the wave propagation results obtained with the viscosities of 0.01 and 1.21×10^{-6} are very close. Then, a viscosity of 0.01 can be approximately used instead of 1.21×10^{-6} to calculate wave propagation. Nevertheless, the real acoustic attenuation in water ($\alpha = 3.35 \times 10^{-7}$) has then to be used in Eq. (38) to get the real acoustic force and real streaming in water. The force thus obtained in water is, however, very low, and, used in Eq. (12), it is not able to generate a flow in the LB simulations, this flow being far too weak. To have a force able to produce acoustic streaming with our LB simulations, we changed the attenuation coefficient used in Eq. (38) to $\alpha = 2.77 \times 10^{-3}$, which is the value obtained for a viscosity $\nu = 0.01$ at $f = 200$ kHz. Such LB simulations will then give the streaming in a more viscous flow than water. To get streaming in water, a possibility would have been to increase the wave frequency f (by a factor of 10 to $f = 2$ MHz, for example), as the attenuation coefficient is proportional to f^2. Many more discretization points, however, would have been necessary for the LB simulations to take into account such high-frequency waves, and this is beyond our numerical possibilities.

The force field calculated with $\nu = 0.01$ and $A = 0.01$ is shown in Fig. 13. In contrast to the results presented in Fig. 10, the force does not weaken too quickly away from the source because the attenuation corresponding to $\nu = 0.01$ is small compared to that associated with $\nu = 0.06$. The global intensity of the force, however, is proportional to α (Eq. (38)) and is expected to be smaller for $\nu = 0.01$ than for $\nu = 0.06$. To still assess the reliability of our code, the force field obtained for $\nu = 0.01$ with the analytical solution and the use of Eq. (38) is given in Fig. 14. We see a very good agreement in terms of intensity and structure with the force field obtained numerically in Fig. 13.

The flow generated by streaming with the force field shown in Fig. 13 has then been simulated by the LB method, using now the bounce-back boundary condition at the east wall. This streaming flow is shown in Figs. 15, 16, and 17. Fig. 15 shows the distribution of the x-component of the velocity in the cavity. Since the east wall is impermeable, the flow induced by the attenuated wave in the central part of the cavity, ahead of the transducer, is blocked by this wall and must return along the north and south horizontal walls, giving two recirculation cells in the cavity. As shown by the transverse profile of the horizontal u velocity taken at $x = L/2$ in Fig. 16, the velocity is maximum in the central part of the cavity along the horizontal centerline and weaker in the returning zones along each horizontal wall. The global structure of the flow induced by acoustic streaming is shown with the velocity vector plot in Fig. 17. We see that the two recirculation cells are perfectly symmetric with respect to the horizontal centerline of the cavity and that they are mainly intense in the first half of the cavity.

With the viscosity $\nu = 0.01$, the streaming obtained is still weak and the main flow does not reach the east wall where very low velocities are found. In order to have stronger streaming, the acoustic force can be further increased. For a fixed frequency (200 kHz), we can still increase the acoustic

attenuation coefficient or increase the amplitude of the wave. We now choose to keep $\nu = 0.01$ and to increase the amplitude value from 0.01 to 0.1. Note that the value of the amplitude has to remain low (clearly below 1, i.e. corresponding to $\rho' \ll \rho_0$) to avoid the effect of non-linearity in the acoustic model described in Eq. (31). Figs. 18 and 19 show that, for this new amplitude, the flow in the cavity, still symmetric with respect to the horizontal centerline, becomes more intense, with the recirculation cells almost occupying the whole cavity.

6. Conclusions

The objective of this work was to simulate waves propagation and acoustic streaming in water by the lattice Boltzmann method (LB method). The numerical study presented here has first shown that the LB method can be used to simulate the acoustic waves generated in water by a rectangular acoustic source at $f = 200$ kHz. The proposed numerical model presents a good accuracy, confirmed by the comparison with the analytical calculation. This validation is carried out using the mathematical expression of the density given by the wave equation solution for the case of cylindrical waves emitted by point sources. Another characteristic of the problem, which is important for the calculation of acoustic streaming, is the acoustic force field generated by the attenuated wave propagation. This force field can be calculated with two formulas: in the first formula based on the mean squared pressure, the acoustic attenuation coefficient is explicitly used, whereas, in the second formula based on the spatial variation of the Reynolds stress, the attenuation is only implicitly effective through the spatial evolution of the acoustic velocities. Our study shows that both formulas can be used for situations with strong attenuation coefficients, but that only the first formula explicitly containing the attenuation coefficient can be used for situations with low attenuation coefficient, as the physical situation in the water we want to consider here. This is due to the fact that such a low attenuation effect is difficultly taken into account with precision in the numerical simulations of wave propagation. Finally, the force field given by the first formula has been used to simulate the acoustic streaming. Due to the impermeable condition imposed at the east end wall, the main streaming flow induced in the central part of the cavity ahead of the transducer has to return on both sides along the horizontal walls. A characteristic flow structure with two recirculating cells is thus obtained. This flow is symmetric with respect to the horizontal centerline and increases in intensity when the vibration amplitude is increased.

Acknowledgments

This collaborative work was supported by the PHC Maghreb Partnership Program no. 36951NG and the Phase 2 PHC Toubkal Program. A grant to J.B. and the support from the P2CHPD of the University Claude Bernard Lyon 1 and the PMCS2I of Ecole Centrale de Lyon for the numerical calculations are also gratefully acknowledged.

References

[1] X. He, L. S. Luo. Theory of the lattice Boltzmann method: From the Boltzmann equation to the lattice Boltzmann equation. Physical review E, 1997, vol. 56, no 6, p. 6811. https://doi.org/10.1103/PhysRevE.56.6811.

[2] U. Frisch, B. Hasslacher, Y. Pomeau. Lattice-gas automata for the Navier-Stokes equation. Physical review letters, 1986, vol. 56, no 14, p. 1505. https://doi.org/10.1103/PhysRevLett.56.1505.

[3] G.R. McNamara, G. Zanetti. Use of the Boltzmann equation to simulate lattice-gas automata.

Physical review letters, 1988, vol. 61, no 20, p. 2332. https://doi.org/10.1103/PhysRevLett.61.2332.

[4] A. A. Mohamad. Lattice Boltzmann Method: Fundamentals and Engineering Applications with Computer Codes (Second Edition). Springer, London, 2019. https://doi.org/10.1007/978-1-4471-7423-3.

[5] T. Krüger, H. Kusumaatmaja, A. Kuzmin, O. Shardt, G. Silva, E.M. Viggen. The lattice Boltzmann method: principles and practice. Springer, Cham, 2017. https://doi.org/10.1007/978-3-319-44649-3.

[6] G.N. Frantziskonis. Lattice Boltzmann method for multimode wave propagation in viscoelastic media and in elastic solids. Physical Review E, 2011, vol. 83, no 6, 066703. https://doi.org/10.1103/PhysRevE.83.066703.

[7] G.S. O'Brien, T. Nissen-Meyer, C.J. Bean. A lattice Boltzmann method for elastic wave propagation in a Poisson solid. Bulletin of the Seismological Society of America, 2012, vol. 102, no 3, p. 1224-1234. https://doi.org/10.1785/0120110191.

[8] Y. Guangwu, C. Yaosong, H. Shouxin. Simple lattice Boltzmann model for simulating flows with shock wave. Physical review E, 1999, vol. 59, no 1, p. 454. https://doi.org/10.1103/PhysRevE.59.454.

[9] S. Xiao. A lattice Boltzmann method for shock wave propagation in solids. Communications in numerical methods in engineering, 2007, vol. 23, no 1, p. 71-84. https://doi.org/10.1002/cnm.883.

[10] X.M. Li, R.C.K. Leung, R.M.C. So. One-step aeroacoustics simulation using lattice Boltzmann method. AIAA journal, 2006, vol. 44, no 1, p. 78-89. https://doi.org/10.2514/1.15993.

[11] S. Marié, D. Ricot, P. Sagaut. Comparison between lattice Boltzmann method and Navier–Stokes high order schemes for computational aeroacoustics. Journal of Computational Physics, 2009, vol. 228, no 4, p. 1056-1070. https://doi.org/10.1016/j.jcp.2008.10.021.

[12] S. H. A. O. Weidong, L. I. Jun. Review of lattice Boltzmann method applied to computational aeroacoustics. Archives of Acoustics, 2019, vol. 44, no 2, p. 215–238. https://doi.org/10.24425/aoa.2019.128486.

[13] J.M. Buick, C.A. Greated, D.M. Campbell. Lattice BGK simulation of sound waves. EPL (Europhysics Letters), 1998, vol. 43, no 3, p. 235. https://doi.org/10.1209/epl/i1998-00346-7.

[14] G. Bres, F. Pérot, D. Freed. Properties of the lattice-Boltzmann method for acoustics. In : 15th AIAA/CEAS Aeroacoustics Conference (30th AIAA Aeroacoustics Conference). 2009. p. 3395. https://doi.org/10.2514/6.2009-3395.

[15] E.M. Salomons, W.J.A. Lohman, H. Zhou. Simulation of sound waves using the lattice Boltzmann method for fluid flow: Benchmark cases for outdoor sound propagation. PloS one, 2016, vol. 11, no 1, p. e0147206. https://doi.org/10.1371/journal.pone.0147206.

[16] D. Haydock, J.M. Yeomans. Lattice Boltzmann simulations of attenuation-driven acoustic streaming. Journal of Physics A: Mathematical and General, 2003, vol. 36, no 20, p. 5683. https://doi.org/10.1088/0305-4470/36/20/322.

[17] F. Shan, X. Guo, J. Tu, J. Cheng, D. Zhang. Multi-relaxation-time lattice Boltzmann modeling of the acoustic field generated by focused transducer. International Journal of Modern Physics C, 2017, vol. 28, no 03, 1750038.

[18] M. H. Bouzidi, M. Firdaouss, P. Lallemand. Momentum transfer of a Boltzmann-lattice fluid

with boundaries. Physics of fluids, 2001, vol. 13, no 11, p. 3452-3459. https://doi.org/10.1063/1.1399290.

[19] E.M. Viggen. The lattice Boltzmann method with applications in acoustics. Master's thesis, Norges teknisk-naturvitenskapelige universitet, Fakultet for naturvitenskap og teknologi, Institutt for fysikk, 2009.

[20] H. Xu, P. Sagaut. Optimal low-dispersion low-dissipation LBM schemes for computational aeroacoustics. Journal of Computational Physics, 2011, vol. 230, no 13, p. 5353-5382. https://doi.org/10.1016/j.jcp.2011.03.040.

[21] J. Benhamou, M. Jami, A. Mezrhab, V. Botton, D. Henry. Numerical study of natural convection and acoustic waves using the lattice Boltzmann method. Heat Transfer, 2020, vol. 49, no 6, p. 3779-3796. https://doi.org/10.1002/htj.21800.

[22] A. Carovac, F. Smajlovic, D. Junuzovic. Application of Ultrasound in Medicine. Acta Informatica Medica, 2011, vol. 19, no 3, p. 168. https://doi.org/10.5455/aim.2011.19.168-171.

[23] A.P. Sarvazyan, M.W. Urban, J.F. Greenleaf. Acoustic Waves in Medical Imaging and Diagnostics. Ultrasound in medicine & biology, 2013, vol. 39, no 7, p. 1133-1146. https://doi.org/10.1016/j.ultrasmedbio.2013.02.006.

[24] F.J. Fuchs. Ultrasonic cleaning and washing of surfaces. In : Power ultrasonics. Woodhead Publishing, 2015. p. 577-609. https://doi.org/10.1016/B978-1-78242-028-6.00019-3.

[25] B. Moudjed. Caractérisation expérimentale et théorique des écoulements entraînés par ultrasons. Perspectives d'utilisation dans les procédés de solidification du Silicium Photovoltaïque. Ph.D Thesis, INSA Lyon, 2013.

[26] B. Moudjed, V. Botton, D. Henry, H. Ben Hadid, J.P. Garandet. Scaling and dimensional analysis of acoustic streaming jets. Physics of Fluids, 2014, vol. 26, no 9, 093602. https://doi.org/10.1063/1.4895518.

[27] G. V. Krivovichev. Stability analysis of body force action models used in the single-relaxation-time single-phase lattice Boltzmann method. Applied Mathematics and Computation, 2019, vol. 348, p. 25-41. https://doi.org/10.1016/j.amc.2018.11.056.

[28] C. Eckart. Vortices and streams caused by sound waves. Physical review, 1948, vol. 73, no 1, p. 68. https://doi.org/10.1103/PhysRev.73.68.

[29] L. Rayleigh. On the circulation of air observed in Kundt's tubes, and on some allied acoustical problems. Philosophical Transactions of the Royal Society of London, 1884, vol. 175, p. 1-21. https://doi.org/10.1098/rstl.1884.0002

[30] P. Stansell, C. A. Greated. Lattice gas automaton simulation of acoustic streaming in a two-dimensional pipe. Physics of Fluids, 1997, vol. 9, no 11, p. 3288-3299. https://doi.org/10.1063/1.869443.

[31] D. Haydock, J. M. Yeomans. Lattice Boltzmann simulations of acoustic streaming. Journal of Physics A: Mathematical and General, 2001, vol. 34, no 25, p. 5201. https://doi.org/10.1088/0305-4470/34/25/304.

[32] Y. Rafat, K. Habibi, L. Mongeau. Direct numerical simulations of acoustic streaming in standing wave tubes using the lattice Boltzmann method. In : Proceedings of Meetings on Acoustics ICA2013. Acoustical Society of America, 2013. p. 045006. https://doi.org/10.1121/1.4800937.

[33] J. Lighthill. Acoustic streaming. Journal of sound and vibration, 1978, vol. 61, no 3, p. 391-

418. https://doi.org/10.1016/0022-460X(78)90388-7.

[34] H. Lei, D. Henry, H. Benhadid. Acoustic force model for the fluid flow under standing waves. Applied acoustics, 2011, vol. 72, no 10, p. 754-759. https://doi.org/10.1016/j.apacoust.2011.04.007.

[35] D. D'Humierès. Generalized Lattice-Boltzmann Equations, Rarefied Gas Dynamics: Theory and Simulations. Progress in Astronautics and Aeronautics, 1992, vol. 159, p. 450-458. https://doi.org/10.2514/5.9781600866319.0450.0458

[36] Z. Chai, B. Shi. Multiple-relaxation-time lattice Boltzmann method for the Navier-Stokes and nonlinear convection-diffusion equations: Modeling, analysis, and elements. Physical Review E, 2020, vol. 102, no 2, 023306. https://doi.org/10.1103/PhysRevE.102.023306.

[37] M. Jami, F. Moufekkir, A. Mezrhab, J.P. Fontaine, M. Bouzidi. New thermal MRT lattice Boltzmann method for simulations of convective flows. International Journal of Thermal Sciences, 2016, vol. 100, p. 98-107. https://doi.org/10.1016/j.ijthermalsci.2015.09.011.

[38] A. Mezrhab, M. A. Moussaoui, M. Jami, H. Naji, M. H. Bouzidi. Double MRT thermal lattice Boltzmann method for simulating convective flows. Physics Letters A, 2010, vol. 374, no 34, p. 3499-3507. https://doi.org/10.1016/j.physleta.2010.06.059.

[39] J. Benhamou, S. Channouf, M. Jami, D. Henry, V. Botton. Three-dimensional lattice Boltzmann model for acoustic waves emitted by a source. International Journal of Computational Fluid Dynamics, 2021, p. 1-22. https://doi.org/10.1080/10618562.2021.2019226

[40] M.Y. Gokhale, I. Fernandes. Simulation of forced convection in non-Newtonian fluid through sandstones. International Journal for Computational Methods in Engineering Science and Mechanics, 2017, vol. 18, no 6, p. 302-308. https://doi.org/10.1080/15502287.2017.1366596.

[41] Z. Guo, C. Zheng, B. Shi. Discrete lattice effects on the forcing term in the lattice Boltzmann method. Physical review E, 2002, vol. 65, no 4, 046308. https://doi.org/10.1103/PhysRevE.65.046308.

[42] Z. Chai, T.S. Zhao. Effect of the forcing term in the multiple-relaxation-time lattice Boltzmann equation on the shear stress or the strain rate tensor. Physical Review E, 2012, vol. 86, no 1, 016705. https://doi.org/10.1103/PhysRevE.86.016705.

[43] X. Shan, H. Chen. Lattice Boltzmann model for simulating flows with multiple phases and components. Physical review E, 1993, vol. 47, no 3, p. 1815. https://doi.org/10.1103/PhysRevE.47.1815.

[44] X. Shan, H. Chen. Simulation of nonideal gases and liquid-gas phase transitions by the lattice Boltzmann equation. Physical Review E, 1994, vol. 49, no 4, p. 2941. https://doi.org/10.1103/PhysRevE.49.2941.

[45] A.A. Mohamad, A. Kuzmin. A critical evaluation of force term in lattice Boltzmann method, natural convection problem. International Journal of Heat and Mass Transfer, 2010, vol. 53, no 5-6, p. 990-996. https://doi.org/10.1016/j.ijheatmasstransfer.2009.11.014.

[46] N. Jung, H.W. Seo, C.S. Yoo. Two-dimensional characteristic boundary conditions for open boundaries in the lattice Boltzmann methods. Journal of Computational Physics, 2015, vol. 302, p. 191-199. https://doi.org/10.1016/j.jcp.2015.08.044.

[47] D. Heubes, A. Bartel, M. Ehrhardt. Characteristic boundary conditions in the lattice Boltzmann method for fluid and gas dynamics. Journal of Computational and Applied Mathematics, 2014, vol. 262, p. 51-61. https://doi.org/10.1016/j.cam.2013.09.019.

[48] G. Wissocq, N. Gourdain, O. Malaspinas, A. Eyssartier. Regularized characteristic boundary conditions for the Lattice-Boltzmann methods at high Reynolds number flows. Journal of Computational Physics, 2017, vol. 331, p. 1-18. https://doi.org/10.1016/j.jcp.2016.11.037.

[49] E.M. Viggen. The lattice Boltzmann method: Fundamentals and acoustics. Ph.D thesis, Norwegian University of Science and Technology, Trondheim, Norway, 2014.

[50] L.E. Kinsler, A.R. Frey, A.B. Coppens, J.V. Sanders. Fundamentals of Acoustics (4th Edition). John Wiley & sons, New York, 2000.

Table 1
LBM and physical parameters for the propagation of acoustic waves in water.

Material	$c_{ph}(m/s)$	c_{lbm}(D2Q9)	$\nu_{ph}(m^2/s)$	ν_{lbm}	$\rho_{ph}(kg/m^3)$	ρ_{lbm}
Water (20^0C)	1480	$1/\sqrt{3}$	1×10^{-6}	1.21×10^{-6}	1×10^{3}	1

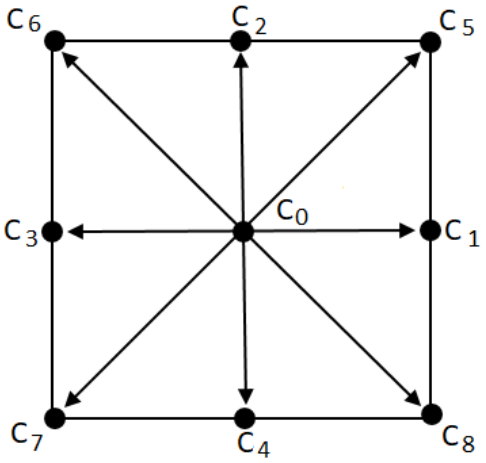

Figure 1. The D2Q9 lattice.

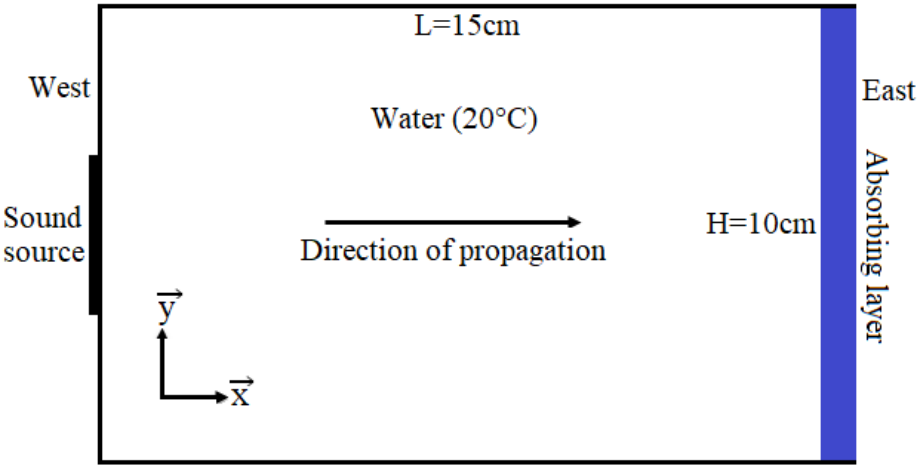

Figure 2. The physical problem studied.

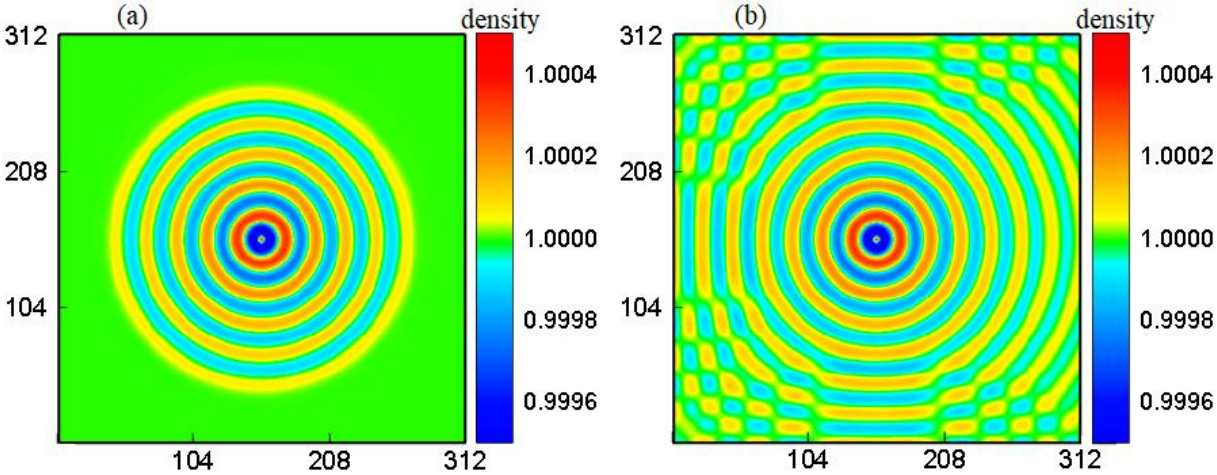

Figure 3. Sound waves propagation in a square cavity at 200 (a) and 400 (b) iterations. A wave absorbing condition is applied at the east wall.

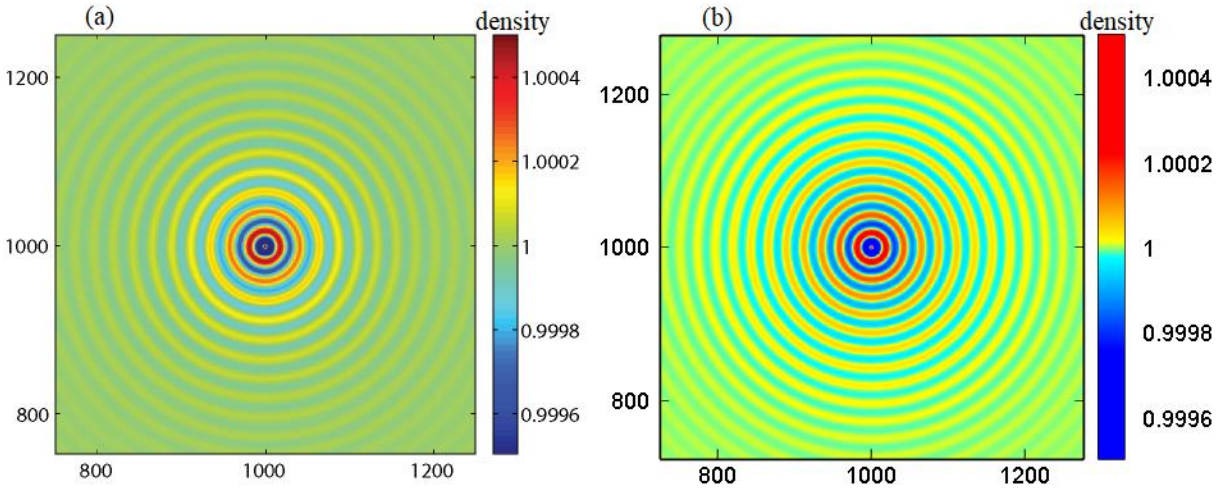

Figure 4. Sound waves propagation in a square cavity: (a) results of the reference [15]; (b) our results.

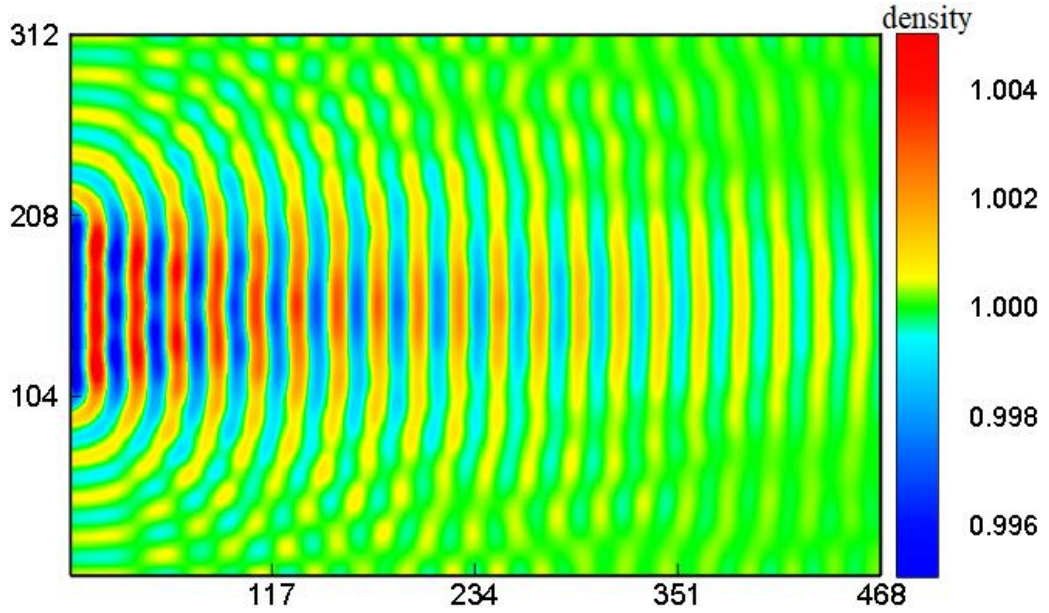

Figure 5. Density field showing sound waves propagation in the rectangular cavity after 1400 iterations for a LBM viscosity $\nu = 1.21 \times 10^{-6}$.

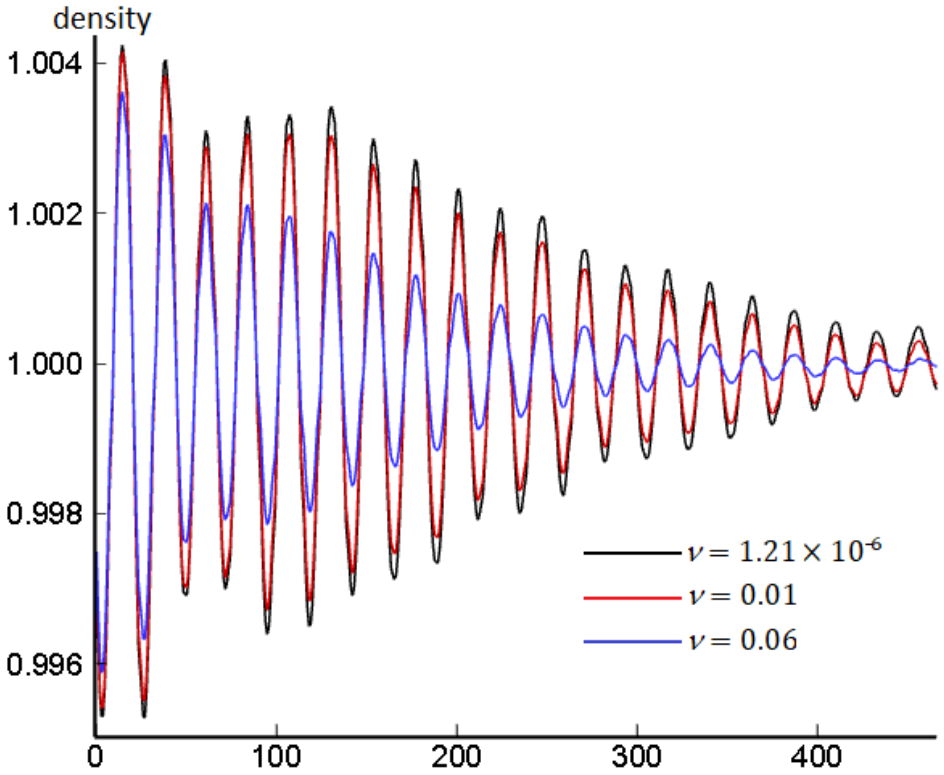

Figure 6. Longitudinal profiles of the fluid density along the x-axis after 1400 iterations and at the position $H/2$ for different values of the LBM viscosity.

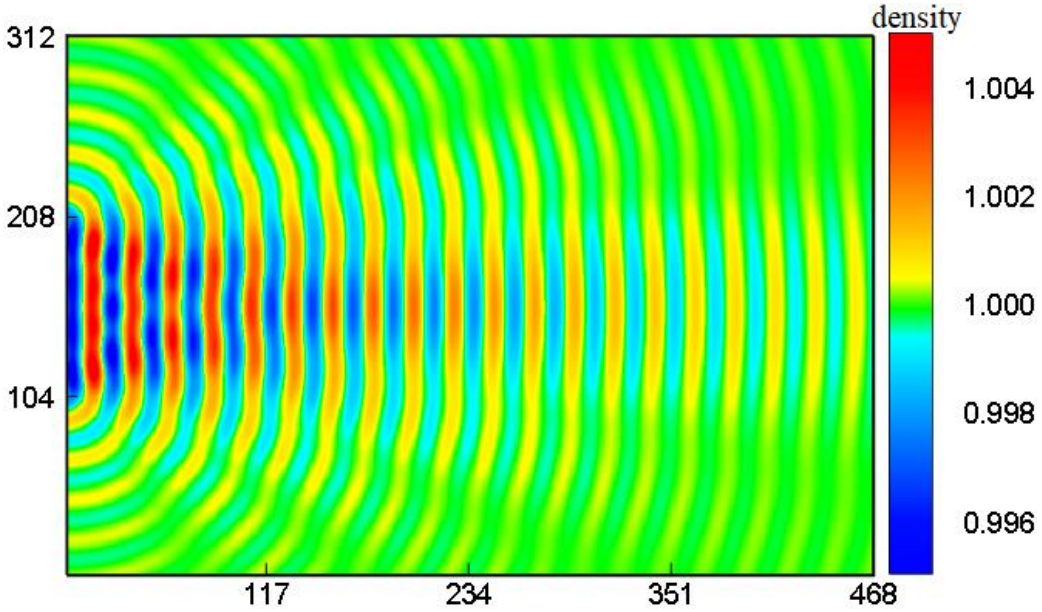

Figure 7. Density field calculated analytically using Eqs. (34) and (35) at $t = 1400\ \Delta t$.

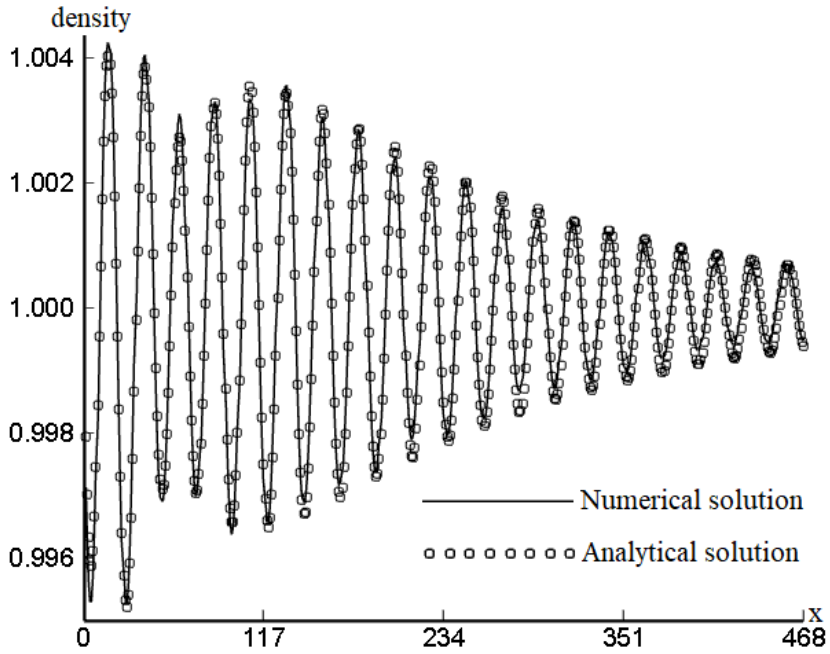

Figure 8. Numerical and analytical longitudinal profiles of the density along the x-axis at $t = 1400\ \Delta t$ and at position $H/2$.

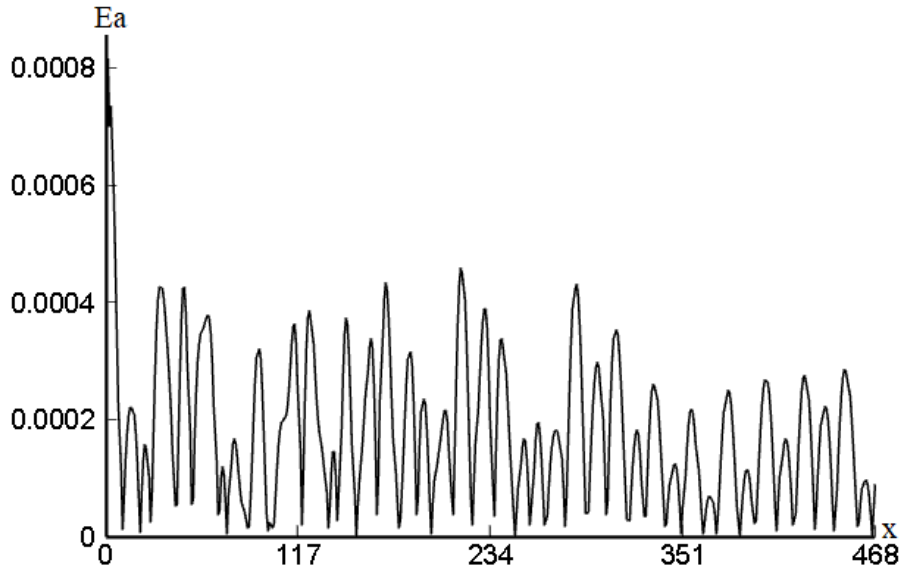

Figure 9. Absolute error variation along the x-axis between the numerical and analytical density profiles presented in Fig. 8.

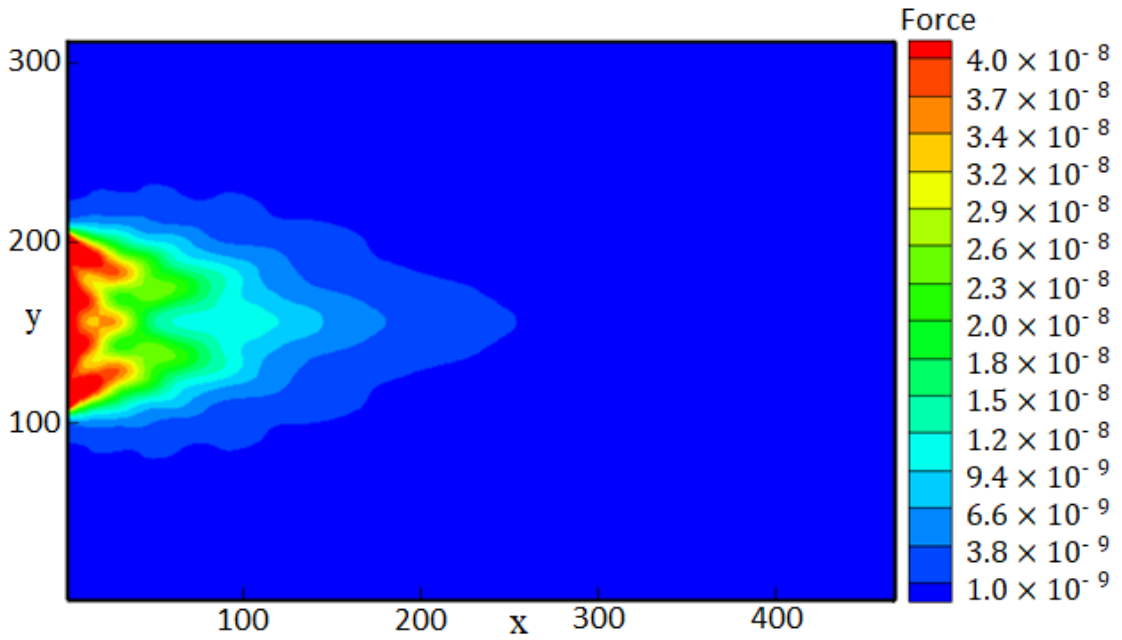

Figure 10. Acoustic force field calculated from Eq. (38) for $\nu = 0.06$.

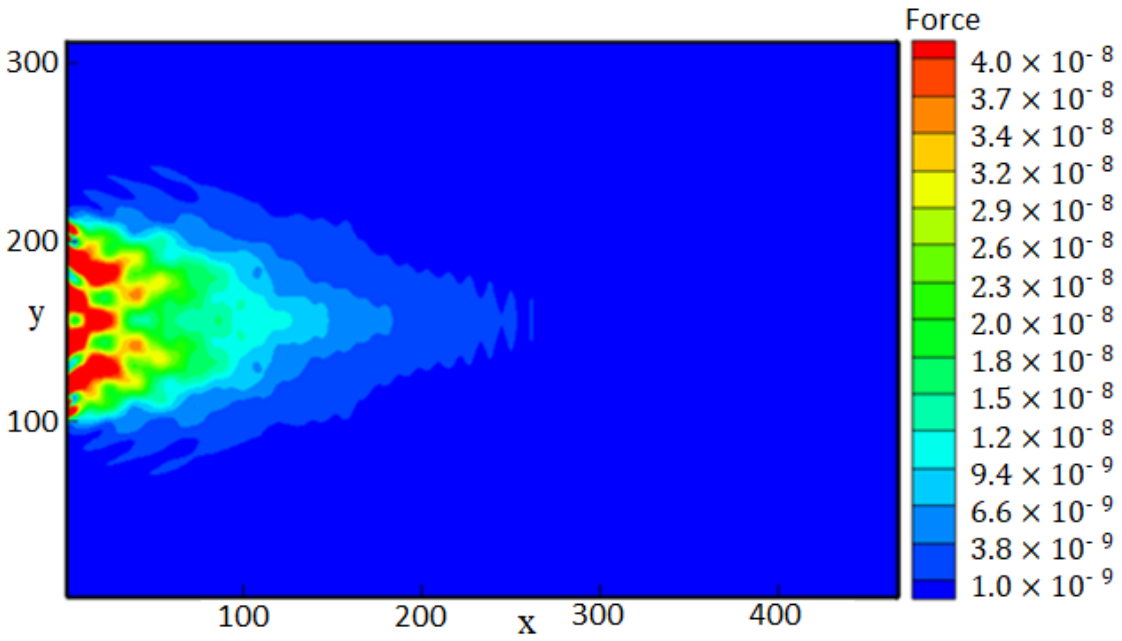

Figure 11. Acoustic force field calculated from Eq. (40) for $\nu = 0.06$.

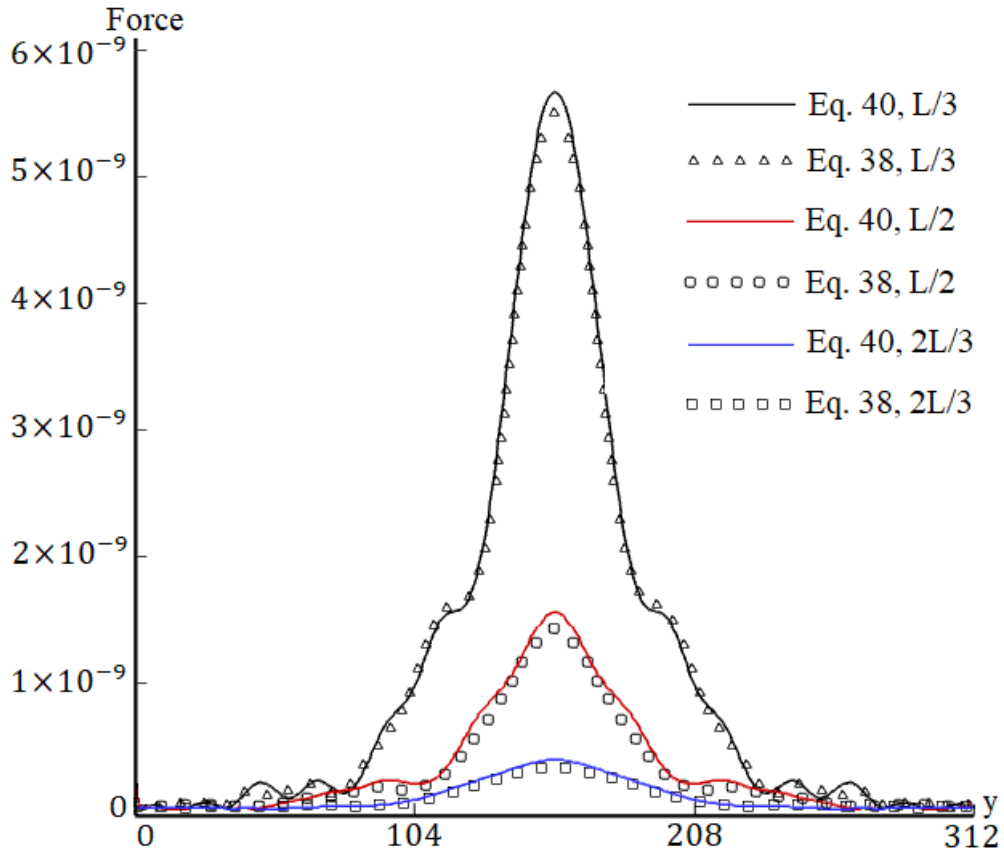

Figure 12. Transverse profiles of the acoustic force calculated by the two different formulas (Eq. (38) or Eq. (40)) at three different positions along the x-axis for $\nu = 0.06$.

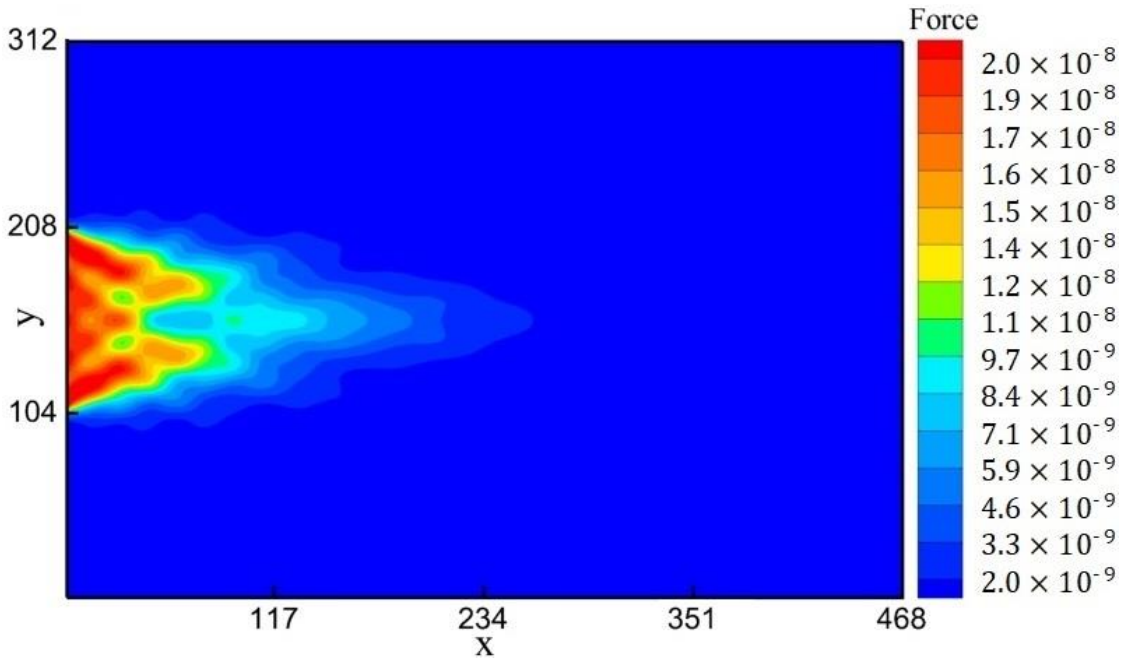

Figure 13. Acoustic force calculated numerically from Eq. (38) for $\nu = 0.01$ ($\alpha = 2.77 \times 10^{-3}$).

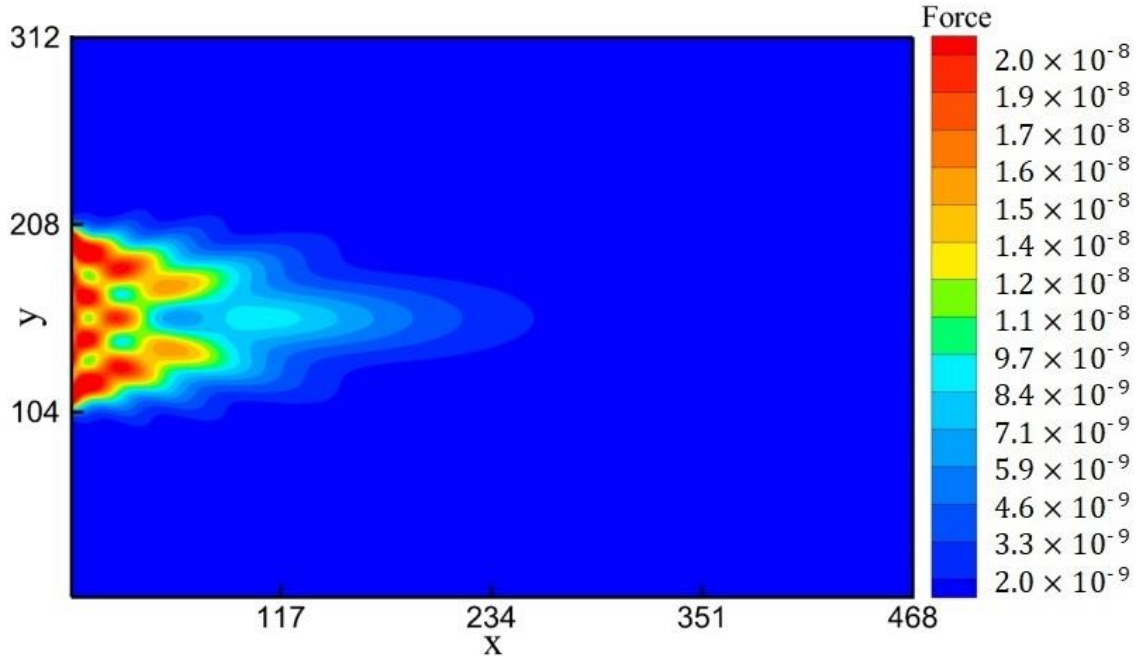

Figure 14. Acoustic force calculated analytically from Eq. (38) for $\nu = 0.01$ ($\alpha = 2.77 \times 10^{-3}$).

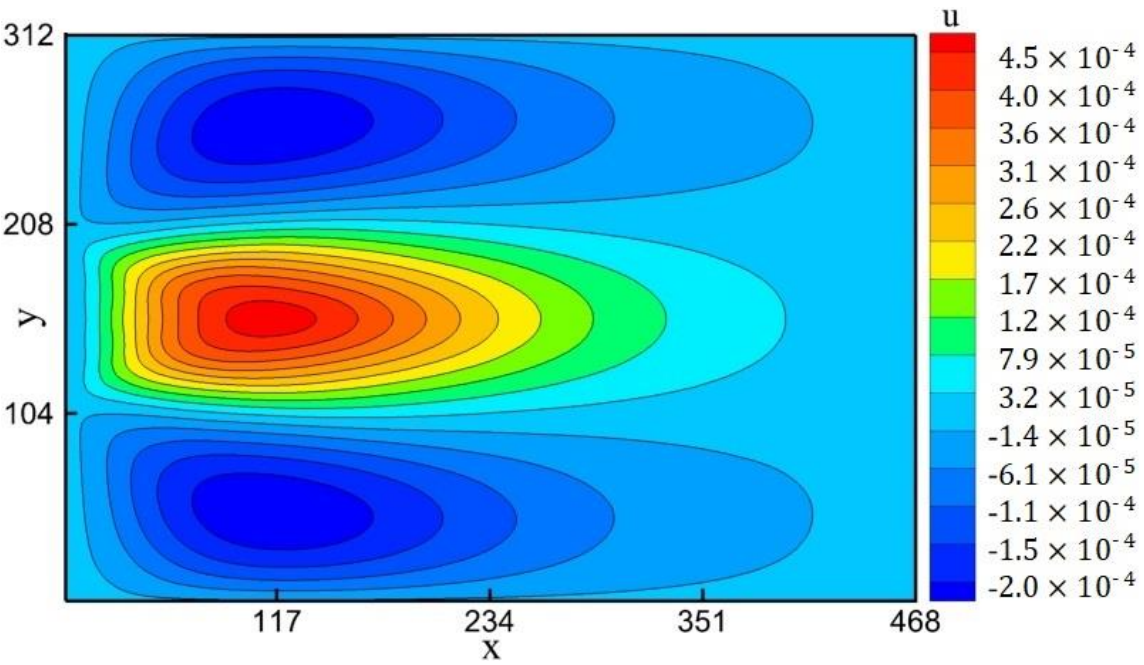

Figure 15. Distribution of the x-component of the velocity for the flow obtained by streaming using the acoustic force described in Eq. (38) with $\nu = 0.01$ and $\mathrm{A} = 0.01$.

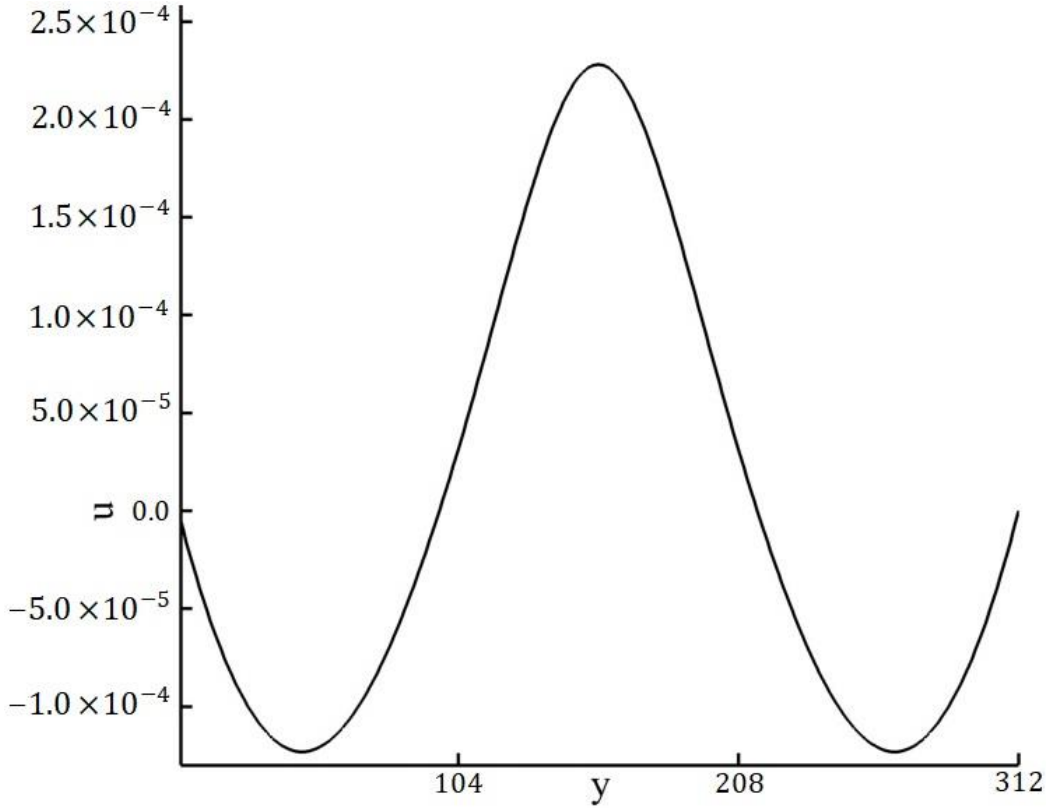

Figure 16. Transverse profile of the u velocity at position $L/2$ for the streaming obtained with $\nu = 0.01$ and $A = 0.01$.

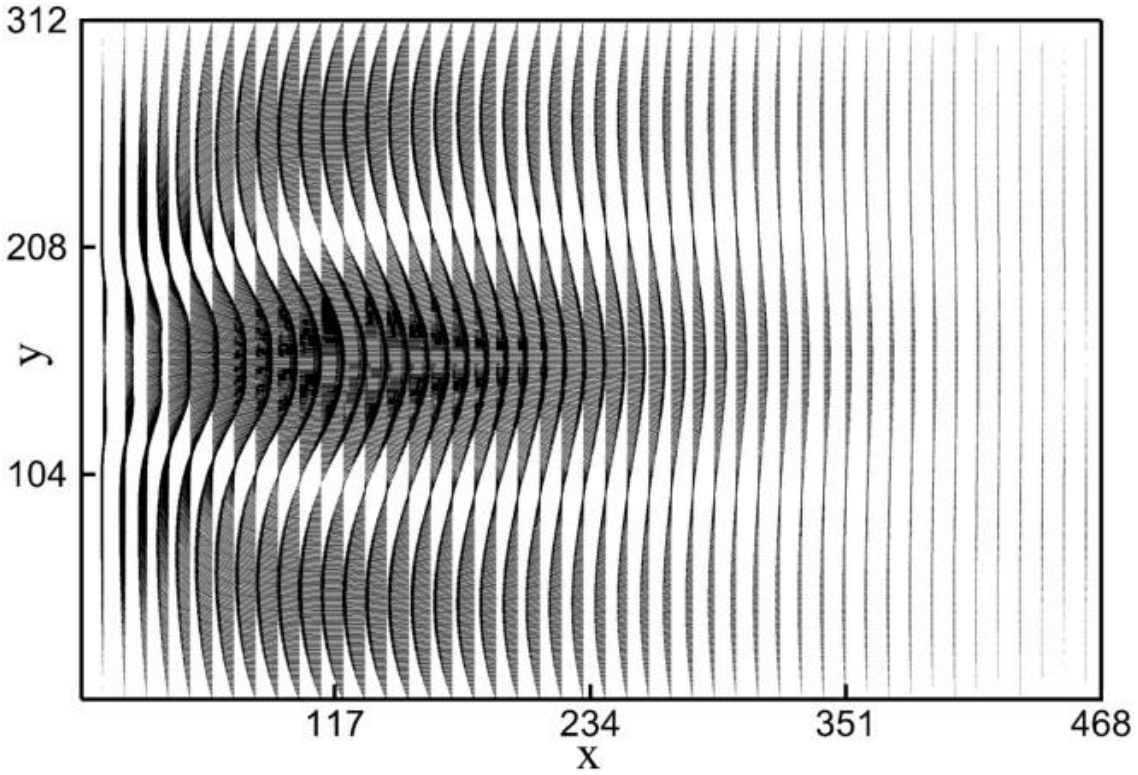

Figure 17. Acoustic streaming produced by the acoustic force described in Eq. (38) using $\nu = 0.01$ and $A = 0.01$.

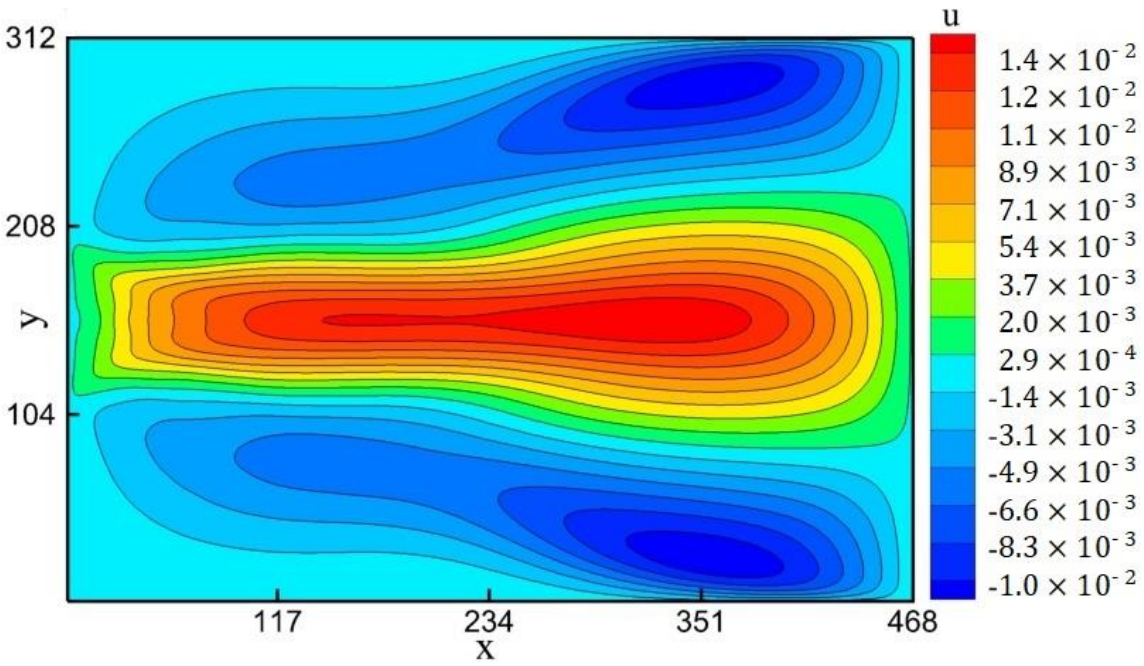

Figure 18. Distribution of the x-component of the velocity for the flow obtained by streaming using the acoustic force described in Eq. (38) with $\nu = 0.01$ and $A = 0.1$.

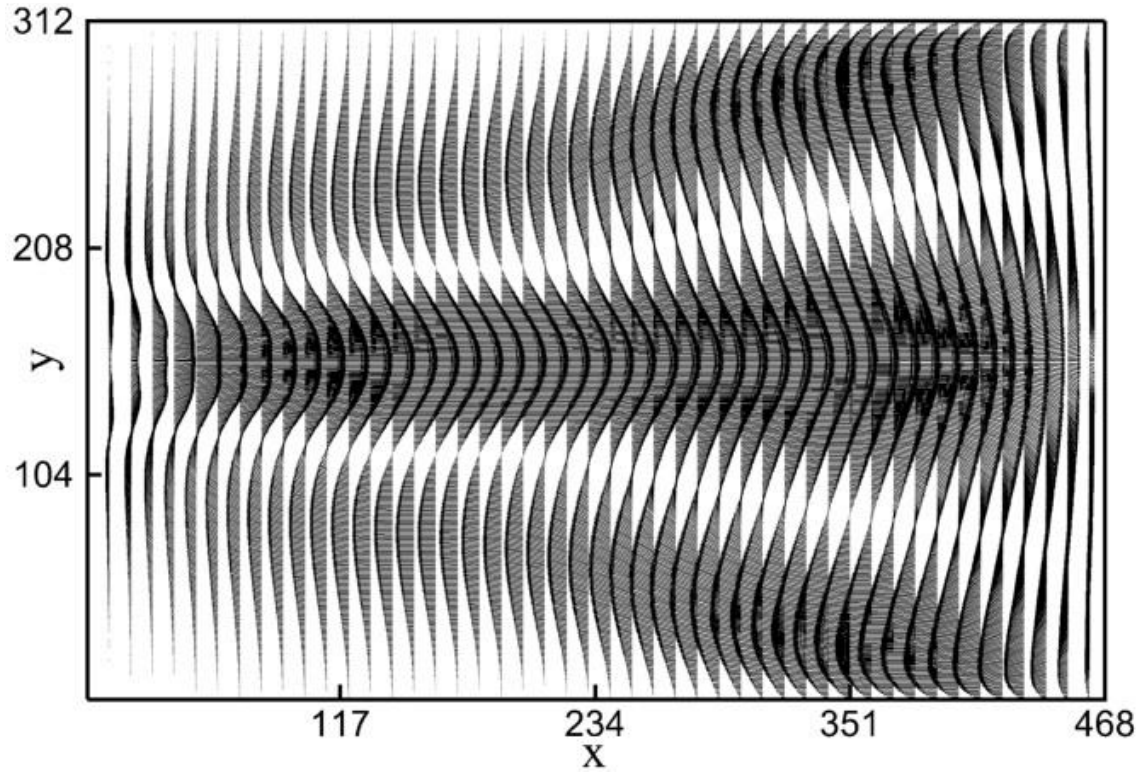

Figure 19. Acoustic streaming produced by the acoustic force described in Eq. (38) using $\nu = 0.01$ and $A = 0.1$.